

Fast Beam Training for Near-Field Communication Systems

Yuan Xu, Chongwen Huang, *Member, IEEE*, Wei Li, Zhaohui Yang, Ahmed Al Hammadi, *Member, IEEE*, Jun Yang, Zhaoyang Zhang, *Senior Member, IEEE*, Chau Yuen, *Fellow, IEEE*, and Mérouane Debbah, *Fellow, IEEE*

Abstract—In millimeter-wave communications, large-scale antenna arrays are commonly employed to mitigate obstacle occlusion and path loss. However, these large-scale arrays generate pencil-shaped beams, which necessitate a higher number of training beams to cover the desired space. This results in the heavy beam training overhead. Furthermore, as the antenna aperture increases, users are more likely to be situated in the near-field region of the base station (BS) antenna array. This motivates our investigation into the beam training problem in the near-field region to achieve efficient beam alignment. To address the high complexity and low identification accuracy of existing beam training techniques, we propose an efficient hashing multi-arm beam (HMB) training scheme for the near-field scenario. Specifically, we first design a set of sparse bases based on the polar domain sparsity of the near-field channel and construct a near-field single-beam training codebook. Then, the hash functions are chosen to construct the near-field multi-arm beam training codebook. Each multi-arm beam training codeword is used in a time slot until the predefined codebook is traversed. Finally, the soft decision and voting methods are applied to distinguish the signal from different BS and obtain the correctly aligned beams. In addition, we provide the logically rigorous proof of computational complexity. Simulation results show that our proposed near-field HMB training method can achieve 96.4% identification accuracy of the exhaustive beam training method and greatly reduce the training overhead to the logarithmic level. Furthermore, we verify its applicability under the far-field scenario as well.

Index Terms—Beam training, sparsity, hashing, multi-arm beam, soft decision, voting mechanism

I. INTRODUCTION

Millimeter-wave (mmWave) technology has emerged as a highly desirable next-generation mobile communication technology due to its numerous advantages. Specifically, it offers higher communication frequencies than conventional frequency bands [1]–[4], which enables the allocation of

a large bandwidth for communication. A large bandwidth is advantageous for data transmission, as it allows for the transmission of more channels or data at the same time, further improving communications throughput [5]. Besides, high frequencies result in short wavelengths, which allow for the use of smaller antennas, making it feasible to deploy large antenna arrays in a relatively small physical space. It is particularly advantageous in the context of Multiple-Input Multiple-Output (MIMO) communication systems [6]–[10].

However, short wavelengths make mmWave signals prone to being absorbed or blocked by obstacles such as buildings, trees, and even rain, resulting in high path loss and low communication coverage [11]–[13]. To mitigate the substantial losses and ensure reliable communication, a promising approach is to use highly directional beams to achieve high gain and spatial resolution. However, this means that the alignment of the transmitter and receiver beams becomes critical. Even small misalignments can result in signal degradation or loss. Typically, beam alignment is achieved by beam scanning techniques, which involves a process where the transmitter and receiver steer the beams to find and maintain the optimal beam alignment.

Nonetheless, high spatial resolution results in a heavy beam training overhead, which is a major concern mmWave systems. In the beam management procedure of the 802.11ad mmWave standard, base stations (BS) typically sweep the entire angular space alternately to establish the aligned beam connections [14]. The overhead associated with beam training is influenced by factors such as spatial resolution, the number of BSs, and the dynamics of the propagation environment [15].

Moreover, a large antenna aperture will make the original far-field region become the near-field region, which is separated by the Rayleigh distance $Z = \frac{2D^2}{\lambda}$ [16]. For example, we consider the carrier frequency to be 28 GHz. When the array aperture for the BS is $D = 0.1$ meters, the Rayleigh distance is only $Z = 1.8$ meters. However, when the array aperture for the large-scale BS increases to $D = 0.3$ meters, the Rayleigh distance can reach $Z = 16.2$ meters. Therefore, users are more likely to be located in the near-field region of the BS antenna array, where far-field beam training methods are not applicable anymore since polarization and distance information must be considered in the near field. To address these difficulties, we focus on near-field beam training and propose an efficient beam training method. In the following, we first review the relevant research works and then summarize our contributions.

Y. Xu, C. Huang, Z. Yang and Z. Zhang are with College of Information Science and Electronic Engineering, Zhejiang University, Hangzhou 310027, China, and with International Joint Innovation Center, Zhejiang University, Haining 314400, China, and also with Zhejiang Provincial Key Laboratory of Info. Proc., Commun. & Netw. (IPCAN), Hangzhou 310027, China (E-mails: {yuan_xu, chongwenhuang, zhaohui_yang, ning_ming}@zju.edu.cn).

L. Wei and C. Yuen are with the School of Electrical and Electronics Engineering, Nanyang Technological University, Singapore 639798 (E-mails: l_wei@ntu.edu.sg, chau.yuen@ntu.edu.sg).

A. Al Hammadi is with the Technology Innovation Institute, 9639 Masdar City, Abu Dhabi, UAE (E-mail: ahmed.alhammadi@tii.ae).

J. Yang is with the State Key Laboratory of Mobile Network and Mobile Multimedia Technology, Shenzhen, 518055, China. J. Yang is also with Wireless Product R&D Institute, ZTE Corporation, Shenzhen 518057, China (E-mail: yang.jun10@zte.com.cn).

M. Debbah is with Department of Electrical Engineering and Computer Science and the KU 6G Center, Khalifa University, Abu Dhabi 127788, UAE (E-mail: Merouane.Debbah@ku.ac.ae).

A. Related works

Beam training in the far field. Accurate channel state information (CSI) is essential for achieving successful beam training. However, due to the variability of the wireless channel, obtaining precise CSI at all times, particularly in low signal-to-noise ratio (SNR) environments, is a challenge [17]. In recent years, researchers have proposed a variety of beam training algorithms to align the directions of received and transmitted beams.

1) *Priori information-assisted beam training* [18]–[24]: this algorithm utilizes environmental priori information such as sensors, dedicated short-range communications (DSRC), and out-of-band information to configure mmWave links [19], and the position information is considered to be a type of side information that can assist in establishing robust links in mmWave wireless communications.

2) *Machine learning-based beam training* [25]–[28]: [25] used a database containing past beam measurements at a specific location to determine the non-line of sight link beam formation direction. [26] proposed a multi-armed bandit framework that can train multiple beam pairs in each attempt. In the multi-armed bandit setup, for arms with a high probability of obtaining a high reward, more attempts are required to obtain a certain cumulative reward.

3) *Blind beam training*: This algorithm does not rely on the priori information or a large amount of data. The exhaustive training method, known as the most precise blind beam training technique, involves selecting the beam corresponding to the dominant path from a predefined codebook by exhaustively enumerating all possible beam combinations between the transmitter and receiver [29]. However, this method necessitates traversing the entire beam space, resulting in significant delays and training overhead [30].

In contrast, the hierarchical training method employs a multi-stage approach, dividing the beam space into two halves at each stage until the desired resolution is achieved [31]. While the hierarchical training method exhibits lower training overhead compared to the exhaustive training method, it has certain drawbacks. Utilizing a wide beam in the early stages can lead to a reduction in beamforming gain. Consequently, at low SNRs, the correct wide beam may not be accurately recognized, and the optimal beam direction may not be ultimately detected. Additionally, this method suffers from inherent error propagation problems [32]. Moreover, since comparative judgments of identification results are required at each stage to determine the training sub-codebooks for subsequent stages, additional delays are introduced as well.

In addition to the single-beam training method, the equal interval multi-arm beam (EIMB) training method utilizes a predetermined sequence of multiple beams, and the aligned beam direction is obtained through ensemble operations after multiple iterations [33]. Compared to the single-beam method, the multi-arm beam training approach offers noticeable advantages in terms of complexity. However, the fixed beam composition may result in persistent leakage interference that cannot be eliminated. Agile-Link is presented in [34], which is a phased-array mmWave system that finds the best beam

alignment without scanning the entire space.

The aforementioned training techniques generally target the far-field region. However, with the substantial increase in the number of mmWave systems antennas, near-field effects are not neglected. In the near-field region, conventional far-field beam training methods experience significant performance degradation. This is mainly due to the absence of angular domain sparsity in the near field, which is a key assumption for the design of far-field beam training codebooks. The proximity effect disrupts the sparsity of the far-field steering vectors, rendering the far-field codebook mismatched with the near-field channel. Consequently, it is necessary to exploit the beam training method by taking full consideration of near-field communication characteristics.

Beam training in the near field. [35] presents a modeling approach that utilizes the near-field scanning method to measure the amplitude and phase of the magnetic field. [36] proposes a novel two-phase beam training method, which decomposes the two-dimensional search into two sequential phases. [37] creating a near-field codebook according to the characteristics of the near-field channel model. Additionally, a corresponding hierarchical near-field beam training scheme is proposed. The analysis in [38] indicates that despite the reduction in array gain, the near-field beam split effect can still contribute to achieving rapid near-field beam training. [39] proposes two deep learning-based near-field beam training schemes, and employs deep residual networks to determine the optimal near-field RIS codeword. [40] trains the deep neural network by performing beam training based on the near-field codebook that contains both angular and distance information, where the optimal angle and distance are jointly predicted with improved. [41] provides an overview of near-field communications and introduces various applications of extremely large-scale arrays in both outdoor and indoor scenarios. It highlights the main design challenges associated with near-field beam training, beam tracking, and beam scheduling. Additionally, promising solutions are proposed to address these challenges.

B. Contributions

The main contribution of this paper is that we propose a low-complexity, high-accuracy hashing multi-arm beam (HMB) training scheme specifically for the near-field scenarios involving multiple transmitters and multiple receivers. For the sake of illustration, we discuss beam training for the downlink in this paper, and it is worth noting that the beam training problem for the uplink can be addressed similarly.

Specifically, we draw the inspiration from the construction principle of far-field discrete Fourier transform (DFT) codebooks. Initially, we define a projection based on the near-field polar domain sparsity. To make this projection analyzable, we employ Taylor binomial expansion, which allows us to express it in a closed-form format. By minimizing this expression, we construct a near-field single-beam training codebook that aims to minimize interference between the training beams. To further enhance performance through multi-arm beam techniques, we employ hash functions and jointly design the antenna responses. This enables us to construct the HMB codebook. During each time slot, each BS selects a multi-arm beam

codeword from the HMB codebook to transmit the signal. Users record their received signals until all the predefined codewords in the HMB codebook have been traversed. Lastly, we apply the soft decision and voting mechanism based on the received signal power to align the beam.

Furthermore, we offer a logically rigorous proof procedure to analyze the training complexity of our proposed method. Simulation results show that our near-field HMB training method achieves a notable enhancement in the identification accuracy of near-field beam training. Specifically, the method achieves a 96.4% accuracy compared to the exhaustive beam training method while significantly reducing the training overhead to the logarithmic level. In addition, we also validate the applicability of our method under far-field conditions.

The rest of the paper is organized as follows. Section II presents the channel and signal models that are relevant to the mmWave communication scenario being investigated. In Section III, we provide a detailed explanation of the near-field single-beam codebook generation method, the process of generating the hashing-based multi-arm beam codebook, the functioning of the decision and voting mechanisms, and a theoretical proof of the complexity. Section IV presents the simulation results, showcasing the performance of the proposed beam training technique. Finally, in Section V, we conclude the paper.

II. SYSTEM MODEL

We consider a downlink mmWave communication scenario where K BSs and U users are distributed in a 3D space. As shown in Fig. 1, the antenna arrays of the BSs are deployed in the xz -plane, each employing a hybrid precoding architecture that equips V radio-frequency (RF) chains and a $M \times N$ antenna uniform planar array (UPA), where $V \ll MN$. Each user device is equipped with a single antenna. The central wavelength, horizontal antenna spacing, vertical antenna spacing, and operating frequency are λ_c , d_x , d_z , and f_c , respectively. The coordinate of the (m, n) -th antenna element of the k -th BS is $(x_{k,n}, y_k, z_{k,m})$, where $x_{k,n} = r_k \cos \theta_k \sin \phi_k + n d_x$, $y_k = r_k \sin \theta_k \sin \phi_k$, $z_{k,m} = r_k \cos \phi_k + m d_z$, $n = 1 - \frac{N+1}{2}, \dots, N - \frac{N+1}{2}$, $m = 1 - \frac{M+1}{2}, \dots, M - \frac{M+1}{2}$. The variables r_k , θ_k and ϕ_k denote the distance, azimuth angle, and elevation angle from the point O' to the BS k , respectively. In the downlink beam training process, the K BSs transmit training symbols in multiple directions while the users listen to the channel in all directions using a quasi-omnidirectional beam. The BS beam alignment requires only the received multi-BS superimposed signal power of each user, while interferences from other users are regarded as noise. Thus, we can train beams for different users separately and simultaneously. For simplicity, we only discuss a typical user.

Let $\mathbf{h}_k \in \mathbb{C}^{MN \times 1}$ denote the channel from the BS k to the user, the received signal y at the user can be expressed as

$$y = \sum_{k=1}^K \mathbf{h}_k^H \mathbf{F}_{RFk} \mathbf{f}_{BBk} x + n_k, \quad (1)$$

where $\mathbf{f}_{BBk} \in \mathbb{C}^{V \times 1}$, $\mathbf{F}_{RFk} \in \mathbb{C}^{MN \times V}$ denote digital precoder and analog beamformer at the k -th BS side, x denotes

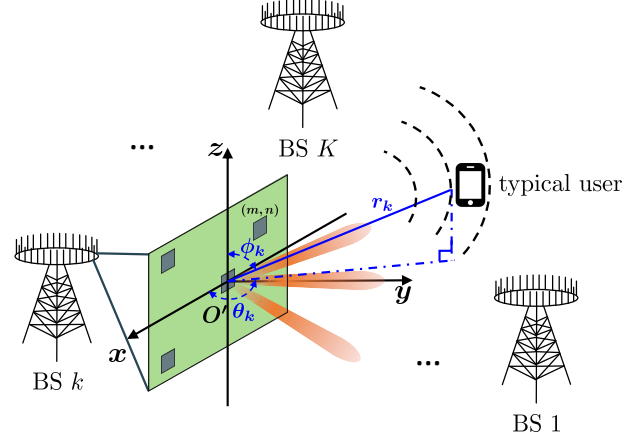


Fig. 1. Downlink mmWave communication scenario with K BSs, and a typical user.

the transmit symbol with power P_0 , $n_k \sim \mathcal{CN}(0, \sigma^2)$ denotes the Gaussian additive white noise.

To represent the channel \mathbf{h}_k more concretely, we start with a review of the near-field properties. Different from the traditional plane wave assumption for the far field, the propagating wavefront of the electromagnetic wave in the near field is approximated as a spherical surface. Moreover, the near field can be divided into the reflected region and the radiated region. Specifically, the former is the near-field region immediately adjacent to the antenna aperture. It is typically defined as $Z < 0.62\sqrt{\frac{2D^2}{\lambda}}$, where D represents the aperture size and λ denotes the wavelength. In this region, no energy is externally radiated since the electric and magnetic fields convert between each other, resulting in energy storage and release. Usually, this region is relatively small, and the wave intensity exponentially decreases with distance.

The latter, which we focus on in this paper, is also named the Fresnel region. It is typically defined as $0.62\sqrt{\frac{2D^2}{\lambda}} < Z < \frac{2D^2}{\lambda}$. In this region, the electromagnetic wave is free from the constraints of the antenna and propagates into space. In addition, its cross-polarised electric field components result in the synthesis of an elliptically polarized wave in a plane parallel to the propagation direction. Thus, it is related to the angular distribution and distance information. In the following, we use the term "near field" to refer to the radiated near field for simplicity.

Based on the spherical wave assumption, the near-field channel can be expressed as

$$\mathbf{h}_k = \sqrt{MN} \sum_{l=1}^L \beta_l e^{-j\psi_l} \mathbf{g}_l, \quad (2)$$

where β_l and ψ_l denote the complex path gain and phase shift of the l -th path. In the line of sight (LoS) link-dominated channel, $\beta_1 \gg \beta_l, l \neq 1$. As a result, we can approximate \mathbf{h}_k as follows

$$\mathbf{h}_k \approx \sqrt{MN} \beta_1 e^{-j\frac{2\pi}{\lambda_c} r_k} \mathbf{g}_1, \quad (3)$$

where $\beta_1 = \frac{\sqrt{\rho_0}}{r_k}$ and ρ_0 represents the reference channel power gain at a distance of 1 meter. The vector \mathbf{g}_1 can be expressed using Eq. (4), and Eq. (5) represents the distance

between the (m, n) -th antenna of the k -th BS and the user. In the near-field region, assuming that $d_x/r_k \ll 1$ and $d_z/r_k \ll 1$, we can approximate the distance $D(m, n)$ using the second-order Taylor expansion [42]. The approximation is given by Eq. (6).

Thus, the phase of \mathbf{g}_1 can be decomposed into two parts that are only related to m and n , respectively. These parts are given by $nd_x \cos \theta_k \sin \phi_k + \frac{n^2 d_x^2 (1 - \cos^2 \theta_k \sin^2 \phi_k)}{2r_k}$ and $md_z \cos \phi_k + \frac{m^2 d_z^2 \sin^2 \phi_k}{2r_k}$. Consequently, we obtain Eq. (7).

The digital precoder of the BS can be expressed as

$$\mathbf{f}_{BB_k} = \frac{1}{\sqrt{V}} [e^{j\vartheta(1)}, \dots, e^{j\vartheta(V)}]^T, \quad (8)$$

where ϑ denotes the adjustment phase vectors of the digital precoder. To obtain the user's position information, we design the beam-aligned observation vector as $\mathbf{a} = \mathbf{F}_{RF_k} \mathbf{f}_{BB_k}$, which can be simply obtained as $\mathbf{a} = \mathbf{g}_1$.

III. NEAR-FIELD CODEBOOK GENERATION

In this section, we focus on addressing the mismatch between the existing far-field codebook and the near-field beam training. To tackle this issue, we begin by designing a single-beam training codebook applicable to the near field. Subsequently, we generate a multi-arm beam training codebook using the hashing method.

A. Near-Field Single-Beam Codebook

In the far field, the scattering paths are limited and the far-field steering vectors are primarily angle-dependent, thus channel sparsity in the angle domain can be achieved by the DFT. By discretizing the angles and using the corresponding discrete Fourier vectors as orthogonal bases, the channel can be transformed to the frequency domain. This transformation facilitates beam training by reducing the interference between training beams. However, the near-field channel model in Eq. (7) reveals that the channel \mathbf{h}_k is nonlinear concerning the antenna subscripts m and n . In contrast to a discrete Fourier vector, \mathbf{h}_k can be jointly described by several far-field Fourier vectors. Consequently, the energy of a near-field path component is not concentrated at a single angle but leaks to multiple adjacent angles [43]. This leakage indicates significant interference between angle-discretized training beams, resulting in substantial performance degradation when the DFT codebook is applied in the near-field beam training.

Even though the near-field channels are not sparse in the angular domain, they are still compressible due to the finite number of paths. To leverage this compressibility, we aim to construct a set of orthogonal bases $\mathbf{a}(\theta_s, \phi_s, r_s) \in \mathbb{C}^{1 \times MN}$ that exhibit sparsity characteristics suitable for the near field. This can be achieved by designing an angle- and distance-sampling approach. The general expression for $\mathbf{a}(\theta_s, \phi_s, r_s)$ is given by Eq. (9), where $D^s(m, n)$ represents the distance from the (m, n) -th antenna of the BS to the sampling point (θ_s, ϕ_s, r_s) .

The principle of distance- and angle-sampling method is to minimize η as small as possible, where

$$\eta \triangleq \max_{p \neq q} f(\theta_p, \theta_q, \phi_p, \phi_q, r_p, r_q), \quad (10)$$

where $f(\theta_p, \theta_q, \phi_p, \phi_q, r_p, r_q) = |\mathbf{a}(\theta_p, \phi_p, r_p) \mathbf{a}(\theta_q, \phi_q, r_q)^H|$ denotes the projection between the two sampled near-field steering vectors. To obtain a closed-form expression, we make an approximation similar to Eq. (6) and obtain Eq. (11) and Eq. (12).

$$f_m \triangleq \frac{1}{M} \sum_{m=-\frac{M-1}{2}}^{\frac{M-1}{2}} e^{j \frac{2\pi}{\lambda_c} g_m(\phi_p, \phi_q, r_p, r_q)} \quad (12)$$

We observe that Eq. (11b) (and similarly in Eq. (11c)) is only related to the index m (n). Besides, when $f_m = 0$, the function $f(\theta_p, \theta_q, \phi_p, \phi_q, r_p, r_q)$ evaluates to zero. Therefore, the goal is to make f_m converge to zero as closely as possible. To achieve this, we can decouple Eq. (11b) into two parts: one part containing only angle information, denoted as $g_m^a \triangleq -md_z(\cos \phi_p - \cos \phi_q)$, and another part containing both angle and distance information, denoted as $g_m^b \triangleq \frac{m^2 d_z^2 \sin^2 \phi_p}{2r_p} - \frac{m^2 d_z^2 \sin^2 \phi_q}{2r_q}$. In the subsequent analysis, we isolate the angular and distance components.

Firstly, considering the case when $g_m^b = 0$, we design the angular sampling method based on g_m^a , which implies that $\frac{\sin^2 \phi}{2r}$ is a constant. In this scenario, the term f_m only depends on g_m^a , which can be expressed as

$$\begin{aligned} f_m &= \frac{1}{M} \sum_{m=-\frac{M-1}{2}}^{\frac{M-1}{2}} e^{j \frac{2\pi m d_z}{\lambda_c} (-md_z(\cos \phi_p - \cos \phi_q))} \\ &= \left| \frac{\sin(\frac{\pi M d_z}{\lambda_c} (\cos \phi_q - \cos \phi_p))}{M \sin(\frac{\pi d_z}{\lambda_c} (\cos \phi_q - \cos \phi_p))} \right|. \end{aligned} \quad (13)$$

It can be found that Eq. (13) is independent of the distances r_p and r_q , which is exactly equivalent to the projection between two far-field steering vectors. The zero points of Eq. (13) satisfy the equation $\cos \phi_q - \cos \phi_p = \frac{2i}{M}$, where $i = 1, \dots, M-1$. Based on this observation, we can sample the angle $\cos \phi_s$ at equal intervals of $\frac{2}{M}$. Specifically, we can set $\cos \phi_s = \frac{2s-M-1}{M}$, where $s = 1, \dots, M$. This angular sampling method ensures that the angles cover the range of possible values for the aligned angle representations.

Afterward, we obtain the distance sampling method based on g_m^b to ensure accurate recovery of the transmitted information x . This is a fundamental difference between the angular domain representation and the polar domain representation. Specifically, the projection $f(\theta_p, \theta_q, \phi_p, \phi_q, r_p, r_q)$ can be expressed as

$$\begin{aligned} &f(\theta_p, \theta_q, \phi_p, \phi_q, r_p, r_q) \\ &= \left| \frac{1}{M} \sum_{m=-\frac{M-1}{2}}^{\frac{M-1}{2}} e^{j \frac{2\pi}{\lambda_c} m^2 d_z^2 (\frac{\sin^2 \phi_p}{2r_p} - \frac{\sin^2 \phi_q}{2r_q})} \right| \\ &\approx \left| \frac{1}{M} \int_{-\frac{M}{2}}^{\frac{M}{2}} e^{j \frac{2\pi}{\lambda_c} m^2 d_z^2 (\frac{\sin^2 \phi_p}{2r_p} - \frac{\sin^2 \phi_q}{2r_q})} dm \right|. \end{aligned} \quad (14)$$

By substituting

$$t = \sqrt{\frac{2(\frac{\sin^2 \phi_p}{2r_p} - \frac{\sin^2 \phi_q}{2r_q})}{\lambda_c}} m d_z, \quad (15a)$$

$$\mathbf{g}_1 = \frac{1}{\sqrt{MN}} [e^{-j\frac{2\pi}{\lambda_c}(D(-\frac{M-1}{2}, -\frac{N-1}{2})-r_k)}, \dots, e^{-j\frac{2\pi}{\lambda_c}(D(m,n)-r_k)}, \dots, e^{-j\frac{2\pi}{\lambda_c}(D(\frac{M-1}{2}, \frac{N-1}{2})-r_k)}]^T \quad (4)$$

$$D(m, n) = \sqrt{(r_k \cos \theta_k \sin \phi_k + nd_x)^2 + (r_k \sin \theta_k \sin \phi_k)^2 + (r_k \cos \phi_k + md_z)^2} \quad (5)$$

$$\begin{aligned} D(m, n) &= \sqrt{r_k^2 + n^2 d_x^2 + m^2 d_z^2 + 2r_k n d_x \cos \theta_k \sin \phi_k + 2r_k m d_z \cos \phi_k} \\ &\approx r_k + nd_x \cos \theta_k \sin \phi_k + \frac{n^2 d_x^2 (1 - \cos^2 \theta_k \sin^2 \phi_k)}{2r_k} + md_z \cos \phi_k + \frac{m^2 d_z^2 \sin^2 \phi_k}{2r_k} \end{aligned} \quad (6)$$

$$\mathbf{g}_1 = \mathbf{v}_x(\theta, \phi, r) \otimes \mathbf{v}_z(\phi, r) \quad (7a)$$

$$[\mathbf{v}_x(\theta, \phi, r)]_n = e^{-j\frac{2\pi}{\lambda_c}(nd_x \cos \theta_k \sin \phi_k + \frac{n^2 d_x^2 (1 - \cos^2 \theta_k \sin^2 \phi_k)}{2r_k})} \quad (7b)$$

$$[\mathbf{v}_z(\phi, r)]_m = e^{-j\frac{2\pi}{\lambda_c}(md_z \cos \phi_k + \frac{m^2 d_z^2 \sin^2 \phi_k}{2r_k})} \quad (7c)$$

$$\mathbf{a}(\theta_s, \phi_s, r_s) = \frac{1}{\sqrt{MN}} [e^{j\frac{2\pi}{\lambda_c}(D^s(-\frac{M-1}{2}, -\frac{N-1}{2})-r_s)}, \dots, e^{j\frac{2\pi}{\lambda_c}(D^s(m,n)-r_s)}, \dots, e^{j\frac{2\pi}{\lambda_c}(D^s(\frac{M-1}{2}, \frac{N-1}{2})-r_s)}] \quad (9a)$$

$$D^s(m, n) = \sqrt{(nd_x - r_s \cos \theta_s \sin \phi_s)^2 + (r_s \sin \theta_s \sin \phi_s)^2 + (md_z - r_s \cos \phi_s)^2} \quad (9b)$$

$$\begin{aligned} f(\theta_p, \theta_q, \phi_p, \phi_q, r_p, r_q) &= \left| \frac{1}{MN} \sum_{m=1-\frac{M+1}{2}}^{M-\frac{M+1}{2}} \sum_{n=1-\frac{N+1}{2}}^{N-\frac{N+1}{2}} e^{j\frac{2\pi}{\lambda_c}[(D^p(m,n)-r_p)-(D^q(m,n)-r_q)]} \right| \\ &= \left| \frac{1}{MN} \sum_{m=-\frac{M-1}{2}}^{\frac{M-1}{2}} \sum_{n=-\frac{N-1}{2}}^{\frac{N-1}{2}} e^{j\frac{2\pi}{\lambda_c}(g_m(\phi_p, \phi_q, r_p, r_q) + g_n(\theta_p, \theta_q, \phi_p, \phi_q, r_p, r_q))} \right| \\ &= \left| \frac{1}{N} \sum_{n=-\frac{N-1}{2}}^{\frac{N-1}{2}} e^{j\frac{2\pi}{\lambda_c} g_n(\theta_p, \theta_q, \phi_p, \phi_q, r_p, r_q)} \frac{1}{M} \sum_{m=-\frac{M-1}{2}}^{\frac{M-1}{2}} e^{j\frac{2\pi}{\lambda_c} g_m(\phi_p, \phi_q, r_p, r_q)} \right| \end{aligned} \quad (11a)$$

$$g_m(\phi_p, \phi_q, r_p, r_q) = -md_z(\cos \phi_p - \cos \phi_q) + \frac{m^2 d_z^2 \sin^2 \phi_p}{2r_p} - \frac{m^2 d_z^2 \sin^2 \phi_q}{2r_q} \quad (11b)$$

$$\begin{aligned} g_n(\theta_p, \theta_q, \phi_p, \phi_q, r_p, r_q) &= -nd_x(\cos \theta_p \sin \phi_p - \cos \theta_q \sin \phi_q) \\ &+ \frac{n^2 d_x^2 (1 - \cos^2 \theta_p \sin^2 \phi_p)}{2r_p} - \frac{n^2 d_x^2 (1 - \cos^2 \theta_q \sin^2 \phi_q)}{2r_q} \end{aligned} \quad (11c)$$

$$\zeta = \sqrt{\frac{(\frac{\sin^2 \phi_p}{2r_p} - \frac{\sin^2 \phi_q}{2r_q})}{\lambda_c}} M d_z, \quad (15b)$$

calculate the value of ζ_Δ that ensures the projection is less than Δ . Therefore,

$$\left| \frac{\sin^2 \phi_p}{r_p} - \frac{\sin^2 \phi_q}{r_q} \right| \geq \frac{2\lambda_c \zeta_\Delta^2}{M^2 d_z^2}. \quad (17)$$

we have

$$\begin{aligned} &f(\theta_p, \theta_q, \phi_p, \phi_q, r_p, r_q) \\ &= \left| \int_0^\zeta \frac{1}{\zeta} e^{j\frac{\pi}{2} t^2} dt \right| \\ &\stackrel{(a)}{=} \left| \frac{C(\zeta) + jS(\zeta)}{\zeta} \right|, \end{aligned} \quad (16)$$

where the equal sign (a) is due to the fact that $C(x) = \int_0^x \cos(\frac{\pi}{2} t^2) dt$ and $S(x) = \int_0^x \sin(\frac{\pi}{2} t^2) dt$ are Fresnel integrals.

Since the projection $f(\theta_p, \theta_q, \phi_p, \phi_q, r_p, r_q)$ decreases with increasing ζ and approaches 0, we set a threshold Δ , and

If we use the angular sampling method described earlier, and sample the distances according to Eq. (17), then the projection of the two near-field steering vectors will be no larger than Δ . Consequently, we can construct the observation vector \mathbf{a} as orthogonal bases $\mathbf{a}(\theta_s, \phi_s, r_s)$. By doing so, we can extract the signal in the near-field position (θ_s, ϕ_s, r_s) . To accurately capture the near-field signal, we use the collection of $\mathbf{a}(\theta_s, \phi_s, r_s)$ based on all the sampling points to form the near-field single-beam codebook \mathbf{C} , which can be expressed as

$$\mathbf{C} = [\mathbf{a}(\theta_1, \phi_1, r_1); \dots; \mathbf{a}(\theta_S, \phi_S, r_S)]. \quad (18)$$

It is worth noting that the codebook construction method described above can also be applied to the far-field region when the distance sampling r_s tends to infinity. It can be seen in the simulation results that the codebook constructed using this method has comparable performance to that of the DFT codebook.

B. Hashing Multi-Arm Beam Codebook Generation

To reduce the beam training overhead while maintaining the identification accuracy, we consider the generation of multi-arm beams for training. The multi-arm beams point in multiple directions simultaneously and can be constructed by selecting codewords from the single-beam codebook \mathbf{C} and combining them. The combination can be accomplished by hashing in computer science, by arranging the codewords from the single-beam codebook. Specifically, hashing is a technique commonly employed to store data based on its keyword or other attributes [44]. Here's an outline of the main ideas:

1. Define the universe of keys: We denote the universe of keys as the collection of all codeword indexes $\mathcal{U} = \{0, 1, \dots, N_C - 1\}$, where N_C represents the number of codewords in the single-beam codebook.

2. Define the hash values: We define the interpreted hash values as $\mathcal{T} = \{0, 1, \dots, B - 1\}$, where a hash function $h : \mathcal{U} \rightarrow \mathcal{T}$ maps each key (codeword index) to the interpreted hash value within the desired range.

3. Randomly select hash functions: From a family $\mathcal{H} = \{h_1, h_2, \dots, h_{|\mathcal{H}|}\}$ of hash functions, we randomly select a subset of hash functions to be used in the combination. The family \mathcal{H} consists of distinct hash functions, and $|\mathcal{H}|$ represents the total number of distinct functions in the family. The construction of the family \mathcal{H} is based on the following theorem.

Theorem 1: For the Galois field $GF(N_C)$, we construct a k -wise independent map from \mathcal{U} to \mathcal{T} as follows:

Pick k random numbers $a_0, a_1, \dots, a_{k-1} \in GF(N_C)$. For any $x \in \mathcal{U}$,

$$h(x) \triangleq a_0 + a_1x + a_2x^2 + \dots + a_{k-1}x^{k-1} \bmod B, \quad (19)$$

where the calculations are done over the field $GF(N_C)$, and $|\mathcal{H}| = N_C^k - N_C$, because a_1, a_2, \dots, a_{k-1} cannot equal to zero at the same time.

Proof: Define

$$\begin{bmatrix} 1 & x_1 & x_1^2 & \dots & x_1^{k-1} \\ 1 & x_2 & x_2^2 & \dots & x_2^{k-1} \\ \dots & & & & \\ 1 & x_k & x_k^2 & \dots & x_k^{k-1} \end{bmatrix} \begin{bmatrix} a_0 \\ a_1 \\ a_2 \\ \dots \\ a_{k-1} \end{bmatrix} = \begin{bmatrix} r_1 \\ r_2 \\ \dots \\ r_k \end{bmatrix}. \quad (20)$$

Thus,

$$\begin{bmatrix} a_0 \\ a_1 \\ a_2 \\ \dots \\ a_{k-1} \end{bmatrix} = \begin{bmatrix} 1 & x_1 & x_1^2 & \dots & x_1^{k-1} \\ 1 & x_2 & x_2^2 & \dots & x_2^{k-1} \\ \dots & & & & \\ 1 & x_k & x_k^2 & \dots & x_k^{k-1} \end{bmatrix}^{-1} \begin{bmatrix} r_1 \\ r_2 \\ \dots \\ r_k \end{bmatrix}, \quad (21)$$

where the matrix is invertible because for $\forall i \neq j \in \{1, \dots, k\}$, $x_i \neq x_j$, and matrix inverses are done over the finite field

$GF(N_C)$. This implies that when fixing x_1, x_2, \dots, x_k , there is only a unique set of coefficients a_0, a_1, \dots, a_{k-1} corresponding to r_1, r_2, \dots, r_k , as Eq. (22). The mentioned polynomial serves as a hash function, mapping the elements from the universe \mathcal{U} to itself. To form a family of hash functions that map $\mathcal{U} \rightarrow \mathcal{T}$, we discard $\lceil \log_2 N_C \rceil - \lceil \log_2 B \rceil$ bits from the values r_i . It results in a collection of hash functions that effectively map elements from the universe \mathcal{U} to the interpreted hash values within the designated range $\mathcal{T} = \{0, 1, \dots, B - 1\}$.

The randomly chosen coefficients a_0, a_1, \dots, a_{k-1} make the results of the polynomial follow the uniform distribution. Consequently, the outcomes obtained after applying the modulo operation exhibit the same probability distribution. That is, the probability that $r_i \bmod B$ is equal to a given value $\alpha_i \in \mathcal{T}$ is at most $\frac{1}{B}$. Importantly, when $x_1 \neq x_2 \neq \dots \neq x_k$, we obtain the desired property expressed by Eq. (23), which signifies the attainment of k -wise independence.

Next, we can utilize the hashing results to generate the multi-arm beams. This process involves randomly selecting a hash function from the family \mathcal{H} and computing the hash values of all elements $x \in \mathcal{U}$ which serve as storage addresses. Consequently, each bucket \mathbf{d}_b comprising $R = N_C/B$ keywords represents a multi-arm beam. Thus, we can represent the multi-arm beams generated by hashing as follows:

$$\mathbf{D} = [\mathbf{d}_1; \dots; \mathbf{d}_B], \quad \mathbf{d}_b = [d_b^1, \dots, d_b^R], \quad (24)$$

where commas (,) and semicolons (;) denote the row separators and column separators, respectively.

Fig. 2 illustrates two times hash that hashing the codewords representing 16 directions uniformly into 4 multi-arm beams. Each multi-arm beam encompasses a total of $N_C/B = 4$ distinct directions.

In contrast to the simple antenna partitioning approach [33], we jointly design the response of all antennas to generate the multi-arm beam codebook $\tilde{\mathbf{C}}$ for training. Specifically, for each \mathbf{d}_b , we optimize the digital precoder \mathbf{f}_{BB_k} to map the data stream to the designated RF chain, while the analog beamformer \mathbf{F}_{RF_k} selects $V = R$ codewords from the single-beam codebook \mathbf{C} based on the contained codeword indexes. This selection determines the beams to be transmitted through the designated RF chain. In other words, the analog beamformer controls the directionality and beamforming characteristics of the transmitted signal,

$$\mathbf{f}_{BB_k}^b(i, 1) = \frac{e^{j\theta(i)}}{\sqrt{V}}, \quad i = 1, \dots, V, \quad (25)$$

$$\mathbf{F}_{RF_k}^b(:, i) = \mathbf{C}(\mathbf{d}_b^i, :)^T, \quad i = 1, \dots, V. \quad (26)$$

Therefore, the received power at the user from BS k can be derived as Eq. (27). The normalized multi-arm beam radiation pattern of \mathbf{d}_b is denoted by Eq. (28), while Eq. (29) represents the normalized radiation pattern of the s -th single beam.

Because different near-field single beams interfere with each other in their respective main lobes, the s -th single beam has a main lobe region denoted by $\cos \phi' \in [\cos \phi_s - \frac{1}{M}, \cos \phi_s + \frac{1}{M}]$, $\cos \theta' \in [\cos \theta_s - \frac{1}{N}, \cos \theta_s + \frac{1}{N}]$,

$$r' \in \left[\frac{1 + \frac{r_s \lambda_c \zeta_\Delta^2}{\sin^2 \phi_s M^2 d_z^2}}{\frac{1}{r_s} + \frac{2\lambda_c \zeta_\Delta^2}{\sin^2 \phi_s M^2 d_z^2}}, \frac{1 - \frac{r_s \lambda_c \zeta_\Delta^2}{\sin^2 \phi_s M^2 d_z^2}}{\frac{1}{r_s} - \frac{2\lambda_c \zeta_\Delta^2}{\sin^2 \phi_s M^2 d_z^2}} \right]. \quad (30)$$

$$\begin{aligned} & Pr(h(x_1) = \alpha_1 \wedge h(x_2) = \alpha_2 \wedge \dots \wedge h(x_k) = \alpha_k) \\ &= Pr(r_1 \bmod B = \alpha_1 \wedge r_2 \bmod B = \alpha_2 \wedge \dots \wedge r_k \bmod B = \alpha_k), \quad \alpha_i \neq \alpha_j \in \mathcal{T} \end{aligned} \quad (22)$$

$$Pr(h(x_1) = \alpha_1 \wedge h(x_2) = \alpha_2 \wedge \dots \wedge h(x_k) = \alpha_k) = \frac{1}{B^k}, \quad (23)$$

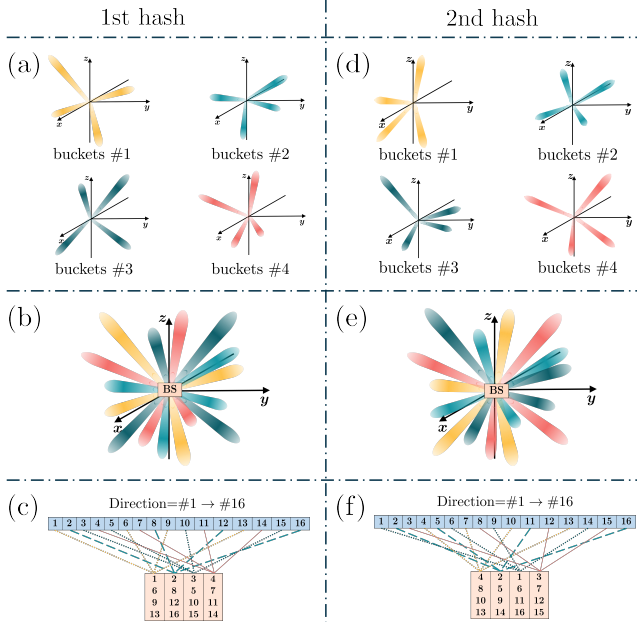


Fig. 2. The schematic diagram for hashing implementation.

We define the unit deviation of $W(r_k, \theta_k, \phi_k, \boldsymbol{\vartheta}, \mathbf{d}_b)$ and $W'(r_k, \theta_k, \phi_k, \mathbf{d}_b^i)$ as Eq. (31). Further, we define the average deviation between the multi-arm beam and single-beam radiation patterns within their respective main lobes as

$$\delta_W(\boldsymbol{\vartheta}, \mathbf{d}_b) \triangleq \frac{1}{V} \sum_{i=1}^V \delta(\boldsymbol{\vartheta}, \mathbf{d}_b^i). \quad (32)$$

Note that when the average deviation $\delta_W(\boldsymbol{\vartheta}, \mathbf{d}_b)$ is sufficiently small, the main lobe of the sub-beam pattern closely resembles the corresponding single beam. In other words, the main lobe characteristics of the single beam are preserved within the multi-arm beam structure. Therefore, we can employ the aforementioned HMB combination \mathbf{d}_b to minimize $\delta_W(\boldsymbol{\vartheta}, \mathbf{d}_b)$ by adjusting $\boldsymbol{\vartheta} = \boldsymbol{\vartheta}_b$ appropriately. This adjustment allows us to generate a well-shaped multi-arm beam, constituting the b -th row of the Hashing multi-arm beam Codebook $\tilde{\mathbf{C}}(b, :) = \mathbf{F}_{RF_k}^b \mathbf{f}_{BB_k}^b$.

IV. NEAR-FIELD BEAM TRAINING

The training process consists of two phases: the scanning phase and the beam identification phase. In the scanning phase, BSs send training symbols using predefined multi-arm beams, each with the same power, until all the predefined multi-arm beams are traversed. In the beam identification phase, we employ a demultiplexing algorithm based on the soft

decision to separate the superimposed signals from multiple BSs. Afterward, we utilize the voting mechanism to obtain aligned beams for each BS.

For a single BS, the soft decision and voting mechanism work as follows. Referring to the first hash illustrated in Fig. 2 (c), if a signal arrives from direction 9, only bucket 1 detects signal energy, while buckets 2, 3, and 4 contain only the noise. This narrows the search space to the directions included in the first multi-arm beam. That is, the potential directions from which the signal originated are 1, 6, 9, and 13. Afterward, a second hashing step is performed, as shown in Fig. 2 (e). As the coefficients of the second hash function are randomized, it is unlikely for the hash results to match those of the previous hash function. In the second hash, only the second bucket exhibits high energy. This indicates that the signal arrives from one of the directions mapped to the third bucket, namely directions 2, 5, 9, and 14. Since the common candidate direction in both the first and second hashes is direction 9, we obtain the 9-th codeword as the aligned beam.

In the case of multiple BSs, to ensure accurate beam training, we employ a total of L rounds of hash. Specifically, BS k randomly selects L distinct hash functions $h_1^k, h_2^k, \dots, h_L^k$ from a predefined family \mathcal{H} to obtain $\mathbf{D}_1^k, \mathbf{D}_2^k, \dots, \mathbf{D}_L^k$. During the scanning phase, BS k transmits training symbols using the codeword from its multi-arm beam codebooks $\tilde{\mathbf{C}}_1^k, \tilde{\mathbf{C}}_2^k, \dots, \tilde{\mathbf{C}}_L^k$. As a result, a total of $Q = BL$ time slots are required for the scanning process, significantly reducing the complexity compared to the traditional method of scanning all BSs. It yields Q received signal power for the typical user, denoted as $\mathbf{P} = [P(1, 1), \dots, P(l, b), \dots, P(L, B)]$. Here, the measurement $P(l, b)$ represents the power of the signal received by the b -th multi-arm beam during the l -th round of hash, corresponding to the $q = (l - 1)B + b$ -th time slot.

$$P(l, b) = \left| \sum_{k=1}^K \mathbf{h}_k^H \mathbf{F}_{RF_k} \mathbf{f}_{BB_k} x + n_k \right|^2 \quad (33)$$

In the following, we introduce the mechanism of the beam identification phase for the multi-BS case.

A. Beam Identification Phase

Suppose the direction of the user to BS k is denoted as $\gamma_k \in \mathcal{U}$. According to Eq. (23), the probability of two arbitrary BSs observing this user simultaneously, i.e., $h_i(\gamma_i) = h_j(\gamma_j)$ for $i \neq j$, is given by $Pr(h_i(\gamma_i) = h_j(\gamma_j)) = \frac{1}{B^2}$. This probability is small enough such that the received signal of each time slot typically contains the signal from at most one BS. Furthermore, due to varying distances between different

$$|y_k|^2(\mathbf{d}_b, \boldsymbol{\vartheta}) \stackrel{(a)}{\approx} |\sqrt{P_0}|\beta_1|\sqrt{MN}e^{-j\frac{2\pi}{\lambda_c}r_k}\sqrt{W(r_k, \theta_k, \phi_k, \boldsymbol{\vartheta}, \mathbf{d}_b)} + n_k|^2 \quad (27)$$

$$W(r_k, \theta_k, \phi_k, \boldsymbol{\vartheta}, \mathbf{d}_b) = \sum_{i=1}^V \frac{1}{V} e^{j\boldsymbol{\vartheta}(i)} \sum_{n=-\frac{N-1}{2}}^{\frac{N-1}{2}} \sum_{m=-\frac{M-1}{2}}^{\frac{M-1}{2}} \frac{1}{MN} e^{-j\frac{2\pi}{\lambda_c}(D\mathbf{d}_b^i(m,n)+D(m,n)-r_{\mathbf{d}_b^i}-r_k)} \quad (28)$$

$$W'(r_k, \theta_k, \phi_k, s) = \sum_{n=-\frac{N-1}{2}}^{\frac{N-1}{2}} \sum_{m=-\frac{M-1}{2}}^{\frac{M-1}{2}} \frac{1}{MN} e^{-j\frac{2\pi}{\lambda_c}(D^s(m,n)+D(m,n)-r_{\mathbf{d}_b^i}-r_k)} \quad (29)$$

$$\delta_W(\boldsymbol{\vartheta}, \mathbf{d}_b^i) \triangleq \int_{r'} \int_{\theta'} \int_{\phi'} \left| \frac{W(r_k, \theta_k, \phi_k, \boldsymbol{\vartheta}, \mathbf{d}_b) - W'(r_k, \theta_k, \phi_k, \mathbf{d}_b^i)}{W'(r_k, \theta_k, \phi_k, \mathbf{d}_b^i)} \right| d\phi d\theta dr \quad (31)$$

BSs and the user, distinct channel gains are obtained. With the same transmit power, it results in distinguishable received signal powers, denoted as $\dot{P}_{m_1} > \dot{P}_{m_2} > \dots > \dot{P}_{m_K}$, where m_k corresponds to the BS with the k -th strongest channel gain. Thus, the demultiplexing algorithm can be designed in conjunction with the soft decision. Specifically, we assign the L time slots with the $(k-1)L+1$ -th $\sim kL$ -th largest value in the received signal power vector \mathbf{P} to BS m_k , which means

$$\mathbf{q}_{m_k} = \arg \max_{(k-1)L+1:kL} \text{descend}(\mathbf{P}), \quad (34)$$

where $\text{descend}(\cdot)$ represents the operation that sorts the vector in descending order. The reason for taking L numbers is that each BS sees the user in only one time slot per round.

Now that we distinguish the received signal power from different BSs, we can proceed with a vote on $\tilde{\mathbf{D}}^k(\mathbf{q}_{m_k}, :)$ to determine γ_k , where colon $(:)$ denotes all the elements of the row/column. In this process, the voting can lead to a unique direction due to the universality property of the hash function family, which implies that for $\forall x \in \mathcal{U}$ and $\forall \alpha \in \mathcal{T}$, the probability $\Pr[h(x) = \alpha]$ is equal to $\frac{1}{B}$. Equivalently, for $\forall x_1, x_2 \in \mathcal{U}$, we have $\Pr[h(x_1) = h(x_2)] = \frac{1}{B}$. Thus, given x_1 and x_2 that satisfy $h_i(x_1) = h_i(x_2)$, we have $\Pr[h_{i'}(x_1) = h_{i'}(x_2)] = \frac{1}{B}$, where $i' \neq i$, $h_i, h_{i'} \in \mathcal{H}$. Moreover, due to the random selection of polynomial coefficients and the distinctness of functions within the hash function family, we can establish Eq. (35).

As a result, the probability of two keywords being hashed to the same address simultaneously by multiple hash functions is sufficiently small. It ensures that multiple rounds of hash make the directions sufficiently dispersed from each other. In other words, based on the randomness of the hash functions, when voting is conducted on arbitrary L beams of the k -th BS, the resulting votes are scattered, and the direction receiving the highest number of votes approximately follows a uniform distribution. However, considering the demultiplexed time slot \mathbf{q}_{m_k} containing the aligned beam, it is highly probable that the direction γ_{m_k} will receive the highest number of votes. This is attributed to the fact that the aligned beam corresponds to the strongest received signal power, and the voting process is designed to identify the dominant direction based on the signal power.

The detailed steps of the beam training are discussed in Algorithm 1. Firstly, in the scanning phase, all BSs simultaneously send training symbols utilizing the predefined multi-arm beams with the same power P_0 , until all the predefined multi-arm beams are traversed. Concurrently, all users listen to the channel using a quasi-omnidirectional beam. In the beam identification phase, we demultiplex the received multi-BS superimposed signal power \mathbf{P}_u at user u using a soft decision approach. This involves assigning the L time slot, determined by the $(k-1)L+1$ -th to kL -th largest values in \mathbf{P}_u , to the corresponding BSs based on their indices, denoted as m_k . Subsequently, we perform a voting process on $\tilde{\mathbf{D}}^k(\mathbf{q}_{m_k}, :)$ to determine the direction γ_k^u with the highest number of votes. Finally, the aligned beam of BS k for user u is selected as the γ_k^u -th codeword in the single beam codebook \mathbf{C} , represented as $\mathbf{C}(\gamma_k^u, :)$.

B. Complexity Analysis

Theorem 2: Given the number of rounds of hash is $L = O(\log M_s)$, it is guaranteed that the probability of identification error is less than $\frac{1}{M_s}$.

Proof:

Lemma 1: (Hoeffding's Lemma) For random variables X , $P(X \in [a, b]) = 1$, $E[X] = 0$, there are

$$\forall s, \quad E[e^{sX}] \leq e^{(s^2(b-a)^2/8)}. \quad (36)$$

Firstly, for the $l \in \{1, \dots, L\}$ -th round of hash, the power of the signal received by the b -th multi-arm beam is denoted as $P(l, b)$, where $q = (l-1)B + b$ represents the time slot number. Since the hash functions for the L rounds of hash are randomly chosen from the hash function family, the values in $\mathcal{L}_b = \{P(1, b), \dots, P(l, b), \dots, P(L, b)\}, \forall b$, are random variables. The number of elements in set \mathcal{L}_b is denoted as $\text{card}(\mathcal{L}_b) = L_b$. Additionally, these variables are independent due to the k -wise independence property.

Furthermore, since the received signal power values are positive and finite, we have $P(l, b) \in [P_{\min}, P_{\max}], l \in \{1, \dots, L\}$, where P_{\min} and P_{\max} represent the upper and lower bounds of the power, respectively. This leads to Eq. (37). The inequality (b) is based on Markov's inequality because the

$$Pr(h_1(x_1) = h_1(x_2) \wedge h_2(x_1) = h_2(x_2) \wedge \dots \wedge h_L(x_1) = h_L(x_2)) = \frac{1}{B^L} \quad (35)$$

$$\forall s, t > 0,$$

$$\begin{aligned} Pr(P(l, b) - E[P(l, b)] \geq t) &= Pr(e^{s(P(l, b) - E[P(l, b)])} \geq e^{st}) \\ &\stackrel{(b)}{\leq} e^{-st} E[e^{s(P(l, b) - E[P(l, b)])}] = e^{-st} \prod_{l=1}^L E[e^{s \frac{P(l, b) - E[P(l, b)]}{L}}] \\ &\stackrel{(c)}{\leq} e^{-st} \prod_{l=1}^L E[e^{s^2 (\frac{P_{max} - P_{min}}{L})^2 / 8}] = e^{-st + \frac{s^2}{8} \sum_{l=1}^L (\frac{P_{max} - P_{min}}{L})^2} \\ &= e^{-st + \frac{s^2 (P_{max} - P_{min})^2}{8L}} \end{aligned} \quad (37)$$

Algorithm 1 HMB Training

Input:

the multi-arm beams for all BSs $\{\mathbf{D}_1^k, \dots, \mathbf{D}_L^k\}_{k=1}^K$
the codebooks $\{\tilde{\mathbf{C}}_1^k, \tilde{\mathbf{C}}_2^k, \dots, \tilde{\mathbf{C}}_L^k\}_{k=1}^K$
the transmit signal x
the number of BSs K
the number of hash rounds L
the number of time slots Q

Output:

the aligned beam indexes $\{\gamma^u\}_{u=1}^U$, $\gamma^u = [\gamma_1^u, \dots, \gamma_K^u]$
the aligned beams of BSs corresponding to users

- 1: **for** $q = 1$ to Q **do**
- 2: \forall BS k transmit x by the q -th multi-arm beam in $\{\tilde{\mathbf{C}}_1^k, \tilde{\mathbf{C}}_2^k, \dots, \tilde{\mathbf{C}}_L^k\}$
- 3: all users record the multi-BS superimposed received signal powers $\{\mathbf{P}_u\}_{u=1}^U$
- 4: **end for**
- 5: **for** (\forall user u) $k = 1$ to K **do**
- 6: $\mathbf{q}_{m_k} = \arg \max_{(k-1)L+1:kL} \text{descend}(\mathbf{P}_u)$
- 7: $\gamma_k^u \leftarrow$ most votes on $\tilde{\mathbf{D}}^k(\mathbf{q}_{m_k}, \cdot)$
- 8: aligned beam of BS k to user u is $\mathbf{C}(\gamma_k^u, \cdot)$
- 9: **end for**

random variable is non-negative and has a finite mean, which satisfies the preconditions of Markov's inequality, (c) is based on Hoeffding's Lemma. Since the index b can take the value from 1 to B , and each multi-arm beam is equivalent due to the randomness of the hash function, we can use the same threshold $E[P(l, b)] \triangleq T_0$. Then we have

$$\frac{P(l, b) - E[P(l, b)]}{L} \in [\frac{P_{min} - T_0}{L}, \frac{P_{max} - T_0}{L}], \quad (38)$$

$$E[\frac{P(l, b) - E[P(l, b)]}{L}] = 0. \quad (39)$$

To obtain the best probability upper bound, we minimize the right-hand side of the equation concerning s , define

$$g(s) = -st + \frac{s^2(P_{max} - P_{min})^2}{8L} = -st + \frac{s^2(\Delta P)^2}{8L}. \quad (40)$$

This equation is a quadratic function that takes the minimum value when $s = \frac{4tL}{(\Delta P)^2}$, thus

$$g(s)_{min} = -\frac{2t^2 L}{(\Delta P)^2}, \quad (41)$$

where $\Delta P \triangleq P_{max} - P_{min}$.

Consequently, we have

$$\forall t > 0, \forall b, \quad Pr(P(l, b) - E[P(l, b)] \geq t) \leq e^{-\frac{2t^2 L}{(\Delta P)^2}}. \quad (42)$$

Because $P(l, b) - E[P(l, b)] = -(E[P(l, b)] - P(l, b))$, in the same way we can obtain

$$\forall t > 0, \forall b, \quad Pr(E[P(l, b)] - P(l, b) \geq t) \leq e^{-\frac{2t^2 L}{(\Delta P)^2}}. \quad (43)$$

Divide the random variable $P(1, b), \dots, P(L, b), \dots, P(L, b)$ into those that contain user signals and those that do not (i.e., only the noise), denote as $\mathcal{L}_b^s = \{P(l, b)^{(s)}\}$ and $\mathcal{L}_b^{ns} = \{P(l, b)^{(ns)}\}$, respectively. We have

$$\mathcal{L}_b^s \in [P_{min}^s, P_{max}^s], \quad E[\mathcal{L}_b^s] \triangleq T_b^s, \quad (44)$$

$$\mathcal{L}_b^{ns} \in [P_{min}^{ns}, P_{max}^{ns}], \quad E[\mathcal{L}_b^{ns}] \triangleq T_b^{ns}, \quad (45)$$

where P_{min}^s, P_{max}^s are the lower and upper bounds of the receive power of the useful signal, $P_{min}^{ns}, P_{max}^{ns}$ are the lower and upper bounds of the received power of the noise.

$$\begin{aligned} \text{card}(\mathcal{L}_b^s) &= L_b^s, \quad \text{card}(\mathcal{L}_b^{ns}) = L_b^{ns}, \\ L_b^s + L_b^{ns} &= L_b. \end{aligned} \quad (46)$$

Since

$$T_b^s L_b^s + T_b^{ns} L_b^{ns} = T_0 L_b, \quad (47)$$

we have $T_b^{ns} < T_0 < T_b^s$.

According to Eq. (42), if we take $t = T_0 - T_b^{ns} > 0$ and

$$L^{ns} = \frac{\ln M_s (P_{max}^{ns} - P_{min}^{ns})^2}{2(T_0 - T_b^{ns})^2}, \quad (48)$$

we have

$$Pr(P(l, b)^{(ns)} \geq T_0) \leq e^{-\frac{2(T_0 - T_b^{ns})^2 L^{ns}}{(P_{max}^{ns} - P_{min}^{ns})^2}} = \frac{1}{M_s}. \quad (49)$$

Similarly, according to Eq. (43), if we take $t = T_b^s - T_0 > 0$ and

$$L^s = \frac{\ln M_s (P_{max}^s - P_{min}^s)^2}{2(T_0 - T_b^s)^2}, \quad (50)$$

we have

$$Pr(P(l, b)^{(s)} \leq T_0) \leq e^{-\frac{2(T_0 - T_b^s)^2 L^s}{(P_{max}^s - P_{min}^s)^2}} = \frac{1}{M_s} \quad (51)$$

$$L^{ns} = O(\log M_s), \quad L^s = O(\log M_s) \quad (52)$$

Eventually, the probability of identification error is reduced to $\frac{1}{M_s}$ when Eq. (52) holds, we obtain

$$L = L^s + L^{ns} = O(\log M_s) \quad (53)$$

Thus, the number of rounds of hash is only related to the desired identification accuracy, a logarithmic level of rounds of hash is sufficient. By using a logarithmic number of rounds, the overhead of HMB training can be significantly reduced compared to the traditional exhaustive beam training.

Here we discuss the advantages of the HMB training. Compared to single beam, multi-arm beam can scan multiple directions simultaneously, greatly reducing the overhead of beams to cover the space. Both the hashing and the equal interval approaches use multi-arm beams. However, the EIMB method uses a predetermined multi-arm beam combination approach as well as a hard decision of threshold comparison, which are the main aspects that differentiate it from our method.

The HMB training employs randomly selected hash functions, which can be perceived as introducing a perturbation to the deterministic combination approach, thereby rendering the combination random. This randomness ensures that the sub-beams are sufficiently dispersed, thereby reducing the impact of leakage interference between sub-beams, particularly after multiple rounds of voting. As in Fig. 2, if there is interference from beam 1 to beam 19 in the first round, there will be no further interference from beam 1 in subsequent rounds because 1 and 9 are no longer in the same multi-arm beam.

By employing an L -round voting mechanism, each round carries equal weight, thus mitigating the influence of errors from individual rounds when L is relatively large. Moreover, since L is complexity dependent, we indicate that L is on the order of $O(\log M_s)$ when the identification error is approximately $1/M_s$. That is, we sacrifice some accuracy compared to the exhaustive approach but greatly reduce the training overhead to $B \log MN$.

Another distinction lies in the use of the soft decision. We consider the relative value, unlike the equal interval method that considers the absolute value. This approach makes it less susceptible to noise and variations in practical power strength. Hence, our method can achieve higher accuracy and greater robustness.

V. SIMULATION RESULTS

We now evaluate the performance of our proposed beam training method with simulation results. The number of BSs and the operating frequency are set to $K = 5$ and $f_c = 28$ GHz respectively, and the signal wavelength is $\lambda_c =$

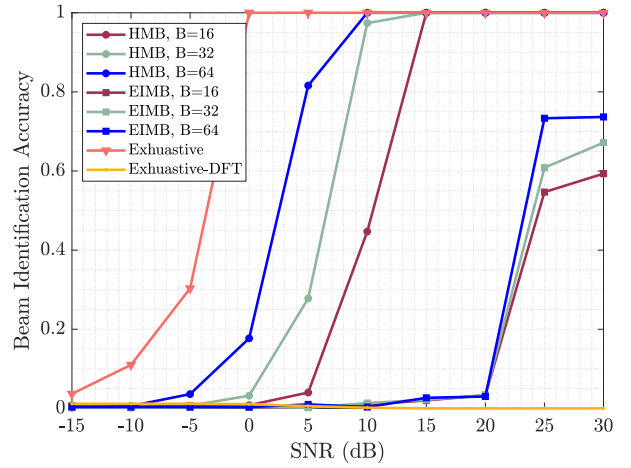


Fig. 3. Success beam identification accuracy versus the SNR.

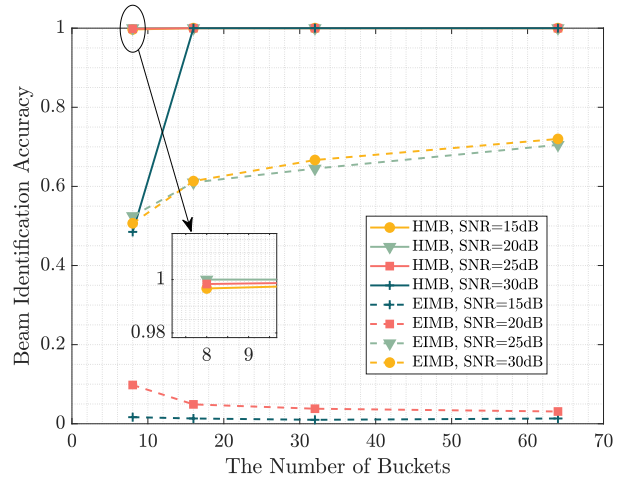


Fig. 4. Success beam identification accuracy versus the number of buckets B at different SNRs.

0.01 m. The planar antenna arrays of BSs contain $M = 4$, $N = 128$ antennas, and the spacing between the antennas is $d_x = d_z = \lambda_c/2$. The reference SNR is $\gamma = \frac{P_0 M N \rho_0}{r_0^2 \sigma^2}$ with $\rho_0 = -72$ dB, $P_0 = 15$ dBm, and $\sigma^2 = -70$ dBm. The achievable rate, denoted in bits/second/Hz (bps/Hz), is given by

$$R = \log_2(1 + \gamma |\mathbf{f}_{BB}^T \mathbf{F}_{RF}^T \mathbf{g}_1|^2). \quad (54)$$

Fig. 3 plots the effect of the SNR on the identification accuracy. We use the exhaustive, EIMB training method with the near-field codebook and exhaustive training with the DFT codebook ("Exhaustive-DFT") as the baseline. Firstly, it can be seen that as the SNR increases, the influence of noise diminishes, leading to improved identification accuracy for all beam training methods. Specifically, the accuracy achieved with the near-field codebook using the exhaustive beam training method converges to 1. However, the accuracy achieved with the far-field codebook is significantly lower, indicating the limitations of the DFT codebook in the near field.

In addition, when utilizing near-field codebooks, it reveals that the HMB training method demonstrates competitive performance compared to the exhaustive training method. Specif-

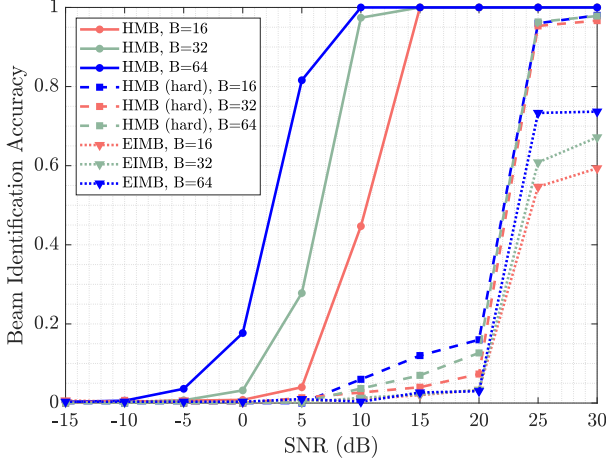


Fig. 5. Success beam identification accuracy versus the SNR when considering soft and hard decisions.

ically, when the number of multi-arm beams $B \geq 32$ and the SNR is not less than 5 dB, the HMB training method can achieve at least 96.4% of the performance achieved by the exhaustive training method. Moreover, even at relatively low SNRs, the HMB training method exhibits considerably improved identification accuracy compared to the EIMB training method.

Fig. 4 plots the effect of the number of buckets on the identification accuracy. It can be noticed that as the number of multi-arm beams B decreases, the accuracy gradually decreases. The reason is that the number of sub-rays R increases as B decreases, making leakage interference among sub-beams more influential on identification results. It is also observed that a higher SNR is beneficial for beam training. Compared to the EIMB training method, the HMB training method shows an outstanding identification accuracy, which converges almost to 1.

Fig. 5 plots the beam identification accuracy versus the SNR when considering soft and hard decisions. Among the evaluated beam training methods, only the depicted "HMB" method utilizes the soft decision, while the "HMB (hard)" method employs the hard decision based on threshold comparison and the HMB codebook. It can be seen that our proposed HMB training method has the best performance, especially when the SNR is relatively small. Specifically, when the SNR is 10 dB and the number of beams $B = 32$, the utilization of soft decision improves the accuracy by 96.9%.

This improvement is attributed to the fact that the use of multi-arm beams allocates the transmit power to each sub-beam, further reducing the power of the received signal, which is more likely to be drowned in the noise at low SNRs. Consequently, accurately and adaptively determining the threshold for the hard decision becomes challenging. The soft decision, on the other hand, compares relative values, eliminates the need for thresholding and is less affected by noise. In addition, when the SNR exceeds 20 dB, the HMB codebook improves accuracy by 22% compared to the EIMB codebook. This is because the equal interval method has a fixed leakage interference, whereas the randomness of the

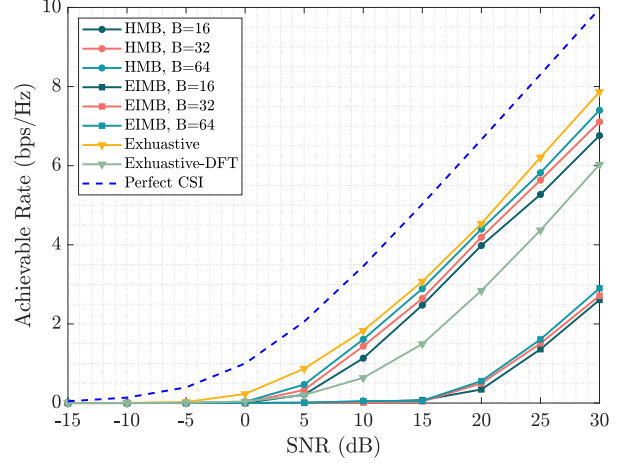


Fig. 6. Achievable rate versus the SNR under different beam training schemes.

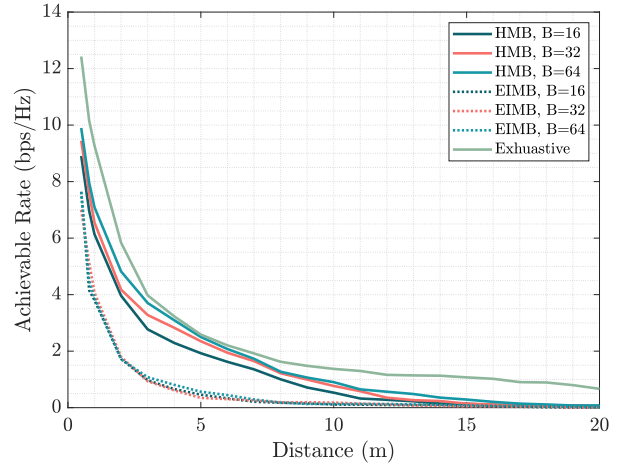


Fig. 7. Achievable rate versus the distance between the BS and the user.

hash adds a random perturbation to the leakage interference between sub-beams, attenuating the effect of this interference on the subsequent decision.

Fig. 6 plots the achievable rate of different beam training methods at different SNRs. It reveals that the achievable rate grows exponentially when the SNR is small, while the growth becomes almost linear as the SNR increases. Among the evaluated methods, the achievable rate of the exhaustive beam training method is closest to the performance of perfect CSI, and the HMB training method achieves 90% of the performance of the exhaustive beam training when $B = 64$. Similarly, it can be observed that both the exhaustive beam training with the DFT codebook and the EIMB training with the designed near-field codebook suffer severe performance losses.

Fig. 7 plots the effect of the BS-user distance on the achievable rate. It can be found that the achievable rate gradually decreases as the distance increases, and faster when the distance is smaller. In addition, the designed HMB training method significantly outperforms the EIMB training method

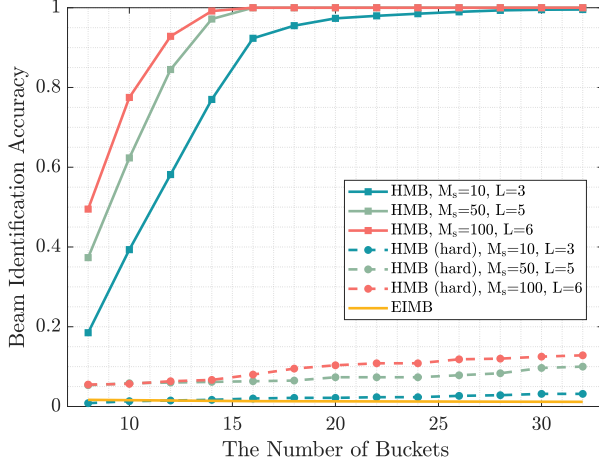


Fig. 8. Success beam identification accuracy versus the number of buckets B for different number of rounds.

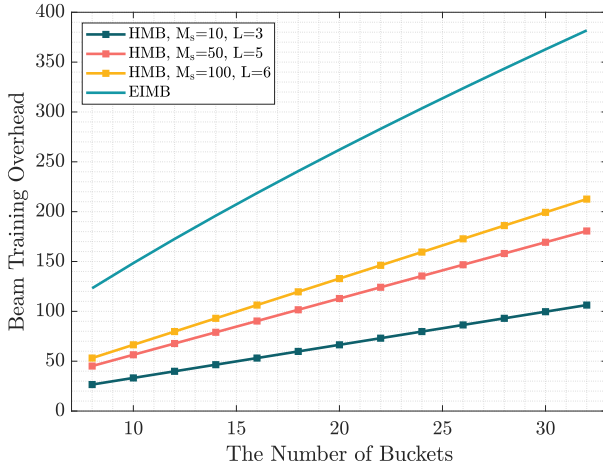


Fig. 9. Training overhead versus the number of buckets B for different number of rounds.

and is infinitely close to the performance of the exhaustive training method.

Fig. 8 and Fig. 9 plot the effect of the number of hash rounds L and buckets B on training accuracy and overhead, respectively. There is a trade-off, a larger L contributes to improved accuracy but introduces extra overhead. It can be found that when the number of buckets B is smaller, it is more beneficial to increase the number of training rounds L . Specifically, when $B = 14$, increasing L from 3 to 5 improves the accuracy by 19.78% while increasing training overhead by 28 time slots, and when $B = 32$ it improves accuracy by only 0.65% while increasing complexity by 64 time slots. Moreover, the accuracy achieved when $L = 3$, with the corresponding $\frac{1}{M_s} = 10\%$, is found to be nearly 90% of the accuracy obtained when $L = 6$ ($\frac{1}{M_s} = 1\%$). This observation serves as a support for the derivation in section IV-B.

Fig. 10 plots the beam identification accuracy versus the SNR under far-field conditions. It can be seen that the codebook constructed using our proposed HMB training method achieves nearly identical accuracy compared to the DFT code-

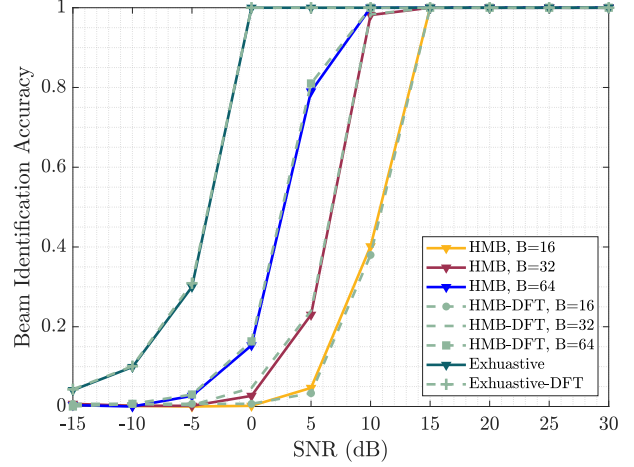


Fig. 10. Success beam identification accuracy versus the SNR under far-field simulation condition.

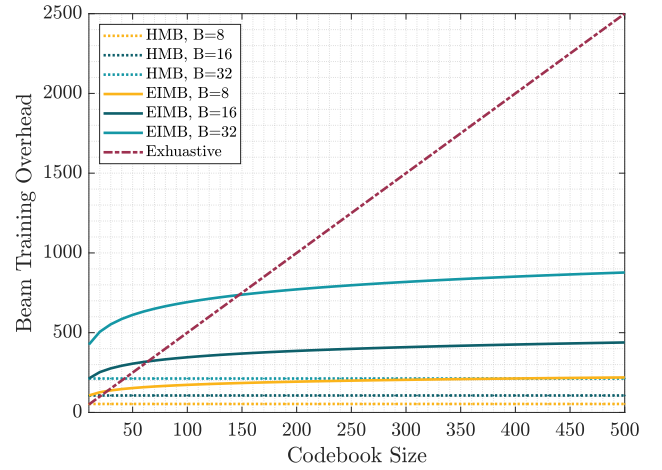


Fig. 11. Training overhead versus codebook size under different beam training schemes.

book, which verifies the applicability of the proposed HMB training method in the far-field region.

Fig. 11 plots the effect of different codebook sizes on the beam training overhead. The exhaustive approach incurs a training time that is directly proportional to the codebook size and the number of BSs K . The training overhead of the EIMB training method is also proportional to K . In contrast, our proposed HMB training method achieves a logarithmic level of training overhead. The training time for HMB is given by $Q = BL = O(B \log MN)$, which is independent of K and significantly reduces the training overhead.

VI. CONCLUSION

In this paper, the HMB training method is proposed for the near field and is verified to be applicable to the far field as well. To begin with, we leverage the polar domain sparsity of the near-field channels to construct near-field training single beams, by minimizing the projection between steering vectors at different sampling points. To further reduce

the overhead of beam training, we use hash functions to generate multi-arm beams. Meanwhile, the soft decision and voting mechanism are employed to improve the identification accuracy and obtain the best-aligned beam. Simulation results show that our proposed beam training method maintains stable and satisfactory performance in terms of beam identification accuracy. It achieves an accuracy of 96.4% compared to the exhaustive training method, while significantly reducing the training overhead to the logarithmic level.

REFERENCES

- [1] F. Khan and Z. Pi, "Mmwave mobile broadband (MMB): Unleashing the 3–300GHz spectrum," in *Proc. 34th IEEE Sarnoff Symp.*, May 2011.
- [2] F. Jameel, S. Wyne, S. J. Nawaz, and Z. Chang, "Propagation channels for mmWave vehicular communications: State-of-the-art and future research directions," *IEEE Wireless Commun.*, vol. 26, no. 1, pp. 144–150, Feb. 2019.
- [3] X. Yang, M. Matthaiou, J. Yang, C. K. Wen, F. Gao, and S. Jin, "Hardware-constrained millimeter-wave systems for 5G: Challenges, opportunities, and solutions," *IEEE Commun. Mag.*, vol. 57, no. 1, pp. 44–50, Jan. 2019.
- [4] Z. Lodro, N. Shah, E. Mahar, S. B. Tirmizi, and M. Lodro, "Mmwave novel multiband microstrip patch antenna design for 5G communication," in *Int. Conf. Comput., Math. Eng. Technol. (iCoMET)*, Jan. 2019.
- [5] A. Ghosh et al., "Millimeter-wave enhanced local area systems: A high-data-rate approach for future wireless networks," *IEEE J. Sel. Areas Commun.*, vol. 32, no. 6, pp. 1152–1163, June 2014.
- [6] M. Sefu, A. Zappone, and E. A. Jorswieck, "Energy efficiency of mmWave MIMO systems with spatial modulation and hybrid beamforming," *IEEE Trans. Green Commun. Networking*, vol. 4, no. 1, pp. 95–108, Mar. 2020.
- [7] R. W. Heath, N. González-Prelcic, S. Rangan, W. Roh, and A. M. Sayeed, "An overview of signal processing techniques for millimeter wave MIMO systems," *IEEE J. Sel. Top. Signal Process.*, vol. 10, no. 3, pp. 436–453, Apr. 2016.
- [8] Y. Katayama, K. Takano, Y. Kohda, N. Ohba, and D. Nakano, "Wireless data center networking with steered-beam mmWave links," in *IEEE Wirel. Commun. Networking Conf. (WCNC)*, 2011.
- [9] M. Hashemi, A. Sabharwal, C. Emre Koksall, and N. B. Shroff, "Efficient beam alignment in millimeter wave systems using contextual bandits," in *Proc IEEE INFOCOM*, 2018.
- [10] K. S. Yngvesson, T. L. Korzeniowski, Y. S. Kim, E. L. Kollberg, and J. F. Johansson, "The tapered slot antenna—a new integrated element for millimeter-wave applications," *IEEE Trans. Microwave Theory Tech.*, vol. 37, no. 2, pp. 365–374, Feb. 1989.
- [11] S. Kuttu and D. Sen, "Beamforming for millimeter wave communications: An inclusive survey," *IEEE Commun. Surveys Tuts.*, vol. 18, no. 2, pp. 949–973, 2nd Quart. 2016.
- [12] Y. Niu, Y. Lia, D. Jin, L. Su, and A. V. Vasilakos, "A survey of millimeter wave (mmWave) communications for 5G: Opportunities and challenges," *Wireless Netw.*, vol. 21, pp. 2657–2676, Nov. 2015.
- [13] L. Wei, R. Q. Hu, Y. Qian, and G. Wu, "Key elements to enable millimeter wave communications for 5G wireless systems," *IEEE Wireless Commun.*, vol. 21, no. 6, pp. 136–143, Dec. 2014.
- [14] S. Jog, J. Wang, J. Guan, T. Moon, H. Hassanieh, and R. R. Choudhury, "Many-to-many beam alignment in millimeter wave networks," in *Proc. of USENIX NSDI*, 2019.
- [15] V. Va, J. Choi, and R. W. Heath, "The impact of beamwidth on temporal channel variation in vehicular channels and its implications," *IEEE Trans. Veh. Technol.*, vol. 66, no. 6, pp. 5014–5029, June 2017.
- [16] K. T. Selvan and R. Janaswamy, "Fraunhofer and fresnel distances: Unified derivation for aperture antennas," *IEEE Ant. Propag. Mag.*, vol. 59, no. 4, pp. 12–15, Aug. 2017.
- [17] A. Nessa, B. Adhikari, F. Hussain, and X. N. Fernando, "A survey of machine learning for indoor positioning," *IEEE Access*, vol. 8, pp. 214945–214965, Nov. 2020.
- [18] A. Abdelreheem, E. M. Mohamed, and H. Esmail, "Millimeter wave location-based beamforming using compressive sensing," in *Proc. 28th Int. Conf. Microelectron. (ICM)*, Dec. 2016.
- [19] J. Choi, V. Va, N. Gonzalez-Prelcic, R. Daniels, C. R. Bhat, and R. W. Heath, "Millimeter-wave vehicular communication to support massive automotive sensing," *IEEE Commun. Mag.*, vol. 54, no. 12, pp. 160–167, Dec. 2016.
- [20] L. Yan, X. Fang, L. Hao, and Y. Fang, "A fast beam alignment scheme for dual-band HSR wireless networks," vol. 69, no. 4, pp. 3968–3979, Apr. 2020.
- [21] N. González-Prelcic, R. Méndez-Rial, and R. W. Heath, "Radar aided beam alignment in mmWave V2I communications supporting antenna diversity," in *Inf. Theory Appl. Workshop (ITA)*, Jan. 2016.
- [22] A. Ali, N. González-Prelcic, and R. W. Heath, "Estimating millimeter wave channels using out-of-band measurements," in *Inf. Theory Appl. Workshop (ITA)*, Jan. 2016.
- [23] M. Hashemi, C. E. Koksall, and N. B. Shroff, "Out-of-band millimeter wave beamforming and communications to achieve low latency and high energy efficiency in 5G systems," *IEEE Trans. Commun.*, vol. 66, no. 2, pp. 875–888, Feb. 2018.
- [24] A. Alkhateeb, O. El Ayach, G. Leus, and R. W. Heath, "Channel estimation and hybrid precoding for millimeter wave cellular systems," *IEEE J. Sel. Top. Signal Process.*, vol. 8, no. 5, pp. 831–846, Oct. 2014.
- [25] J. C. Aviles and A. Kouki, "Position-aided mm-wave beam training under NLOS conditions," *IEEE Access*, vol. 4, pp. 8703–8714, Nov. 2016.
- [26] W. Chen, Y. Wang, and Y. Yuan, "Combinatorial multi-armed bandit: General framework and applications," in *Int. Conf. Mach. Learn. (ICML)*, Feb. 2013.
- [27] A. Alkhateeb, S. Alex, P. Varkey, Y. Li, Q. Qu, and D. Tujkovic, "Deep learning coordinated beamforming for highly-mobile millimeter wave systems," *IEEE Access*, vol. 6, pp. 37328–37348, June 2018.
- [28] J. Zhang, Y. Huang, J. Wang, X. You, and C. Masouros, "Intelligent interactive beam training for millimeter wave communications," *IEEE Trans. Wireless Commun.*, vol. 20, no. 3, pp. 2034–2048, Mar. 2021.
- [29] Junyi Wang et al., "Beam codebook based beamforming protocol for multi-Gbps millimeter-wave WPAN systems," *IEEE J. Sel. Areas Commun.*, vol. 27, no. 8, pp. 1390–1399, Oct. 2009.
- [30] P. Wang, J. Fang, W. Zhang, Z. Chen, H. Li, and W. Zhang, "Beam training and alignment for RIS-assisted millimeter wave systems: State of the art and beyond," *IEEE Wireless Commun.*, pp. 1–14, Dec. 2022.
- [31] S. Hur, T. Kim, D. J. Love, J. V. Krogmeier, T. A. Thomas, and A. Ghosh, "Millimeter wave beamforming for wireless backhaul and access in small cell networks," *IEEE Trans. Commun.*, vol. 61, no. 10, pp. 4391–4403, Oct. 2013.
- [32] S. Noh, M. D. Zoltowski, and D. J. Love, "Multi-resolution codebook based beamforming sequence design in millimeter-wave systems," in *IEEE Glob. Commun. Conf. (GLOBECOM)*, Dec. 2015.
- [33] C. You, B. Zheng, and R. Zhang, "Fast beam training for IRS-assisted multiuser communications," vol. 9, no. 11, pp. 1845–1849, Nov. 2020.
- [34] H. Hassanieh, O. Abari, M. Rodríguez, M. Abdelghany, D. Katabi, and P. Indyk, "Fast millimeter wave beam alignment," in *Proc. ACM Conf. Special Interest Group Data Commun. (SIGCOMM)*, Aug. 2018.
- [35] Y. Vives-Gilbert, C. Arcambal, A. Louis, F. de Daran, P. Eudeline, and B. Mazari, "Modeling magnetic radiations of electronic circuits using near-field scanning method," *IEEE Trans. Electromagn. Compat.*, vol. 49, no. 2, pp. 391–400, May 2007.
- [36] Y. Zhang, X. Wu, and C. You, "Fast near-field beam training for extremely large-scale array," *IEEE Wireless Commun. Lett.*, vol. 11, no. 12, pp. 2625–2629, Dec. 2022.
- [37] X. Wei, L. Dai, Y. Zhao, G. Yu, and X. Duan, "Codebook design and beam training for extremely large-scale RIS: Far-field or near-field?," *China Commun.*, vol. 19, no. 6, pp. 193–204, June 2022.
- [38] M. Cui, L. Dai, Z. Wang, S. Zhou, and N. Ge, "Near-field rainbow: Wideband beam training for XL-MIMO," *IEEE Trans. Wireless Commun.*, vol. 22, no. 6, pp. 3899–3912, June 2023.
- [39] W. Liu, C. Pan, H. Ren, F. Shu, S. Jin, and J. Wang, "Low-overhead beam training scheme for extremely large-scale RIS in near field," *IEEE Trans. Commun.*, vol. 71, no. 8, pp. 4924–4940, Aug. 2023.
- [40] G. Jiang and C. Qi, "Near-field beam training based on deep learning for extremely large-scale MIMO," *IEEE Commun. Lett.*, vol. 27, no. 8, pp. 2063–2067, Aug. 2023.
- [41] C. You, Y. Zhang, C. Wu, Y. Zeng, B. Zheng, L. Chen, L. Dai, and A. L. Swindlehurst, "Near-field beam management for extremely large-scale array communications," *arXiv e-prints*, p. arXiv:2310.01342, Oct. 2023.
- [42] Y. Liu, Z. Wang, J. Xu, C. Ouyang, X. Mu, and R. Schober, "Near-field communications: A tutorial review," *IEEE Open J. Commun. Soc.*, pp. 1–1, Aug. 2023.
- [43] M. Cui and L. Dai, "Near-field channel estimation for extremely large-scale MIMO with hybrid precoding," in *Proc. IEEE Global Communications Conference (GLOBECOM)*, Dec. 2021.
- [44] J. Wang, T. Zhang, j. song, N. Sebe, and H. T. Shen, "A survey on learning to hash," *IEEE Trans. Pattern Anal. Mach. Intell.*, vol. 40, no. 4, pp. 769–790, Apr. 2018.